PRECONDITIONED RICHARDSON NUMERICAL METHOD FOR THERMAL ANALYSIS IN X-RAY LITHOGRAPHY WITH CYLINDRICAL GEOMETRY

W. Dai and R. Nassar
Mathematics and Statistics, College of Engineering and Science, Louisiana Tech University, Ruston, Louisiana 71272, USA

X-ray lithography is an important technique in microfabrication used to obtain structures and devices with a high aspect ratio. In this study, we develop a three-dimensional numerical method for obtaining the steady state temperature profile in an X-ray irradiation process by using a hybrid finite element–finite difference scheme and a preconditioned Richardson method for the Poisson equation at the microscale. A domain decomposition algorithm is then obtained based on a parallel Gaussian elimination for solving block tridiagonal linear systems. Numerical results show that such a method is efficient.

INTRODUCTION

X-ray lithography is an important technique in microfabrication used to obtain structures and devices with a high aspect ratio [1–18]. The process consists of a mask and a photoresist, such as polymethylmethacrylate (PMMA) deposited on a substrate. The mask layer creates a desired pattern on the photoresist by selectively allowing the transmission of irradiation from an X-ray beam. After exposure, the photoresist is developed to remove the irradiated area, leaving behind an imprint of the pattern in the form of exposed substrate and photoresist walls. The pattern can now be used as a micromold. Electroplating can then be used to fill the mold with a metal. The remaining unexposed part of the photoresist can then be removed by an etchant, leaving the free standing microstructure on the substrate.

For rapid manufacturing of microdevices needed for commercialization, exposure times in minutes from high-flux synchrotron sources may be needed. However, with the higher flux, heating of the photoresist may develop. Hence prediction of the temperature distributions in three dimensions in the different layers (mask, gap, photoresist, and substrate, as shown in Figure 1) and of the potential temperature rise in the resist are essential for determining the effect of high-flux X-ray exposure on distortions in the photoresist due to thermal expansion. Analytic solutions to the system of these differential equations describing the

Received 15 December 1997; accepted 17 June 1998.
This research is supported by a Louisiana Educational Quality Support Fund (LEQSF) grant, Contract No. 72-600792.
Address correspondence to Dr. Weizhong Dai, Department of Mathematics and Statistics, Louisiana Tech. University, Ruston, LA 71272, USA.

Numerical Heat Transfer, Part A, 34:599–616, 1998

1040–7782/98 $12.00 + .00

NOMENCLATURE

h_c	convective heat transfer coefficient	W_0	irradiance
$k_1, k_2,$ k_3, k_4	thermal conductivity	x, y, z	Cartesian coordinates
		Δz	grid size in the z direction
r	radius	μ	absorption coefficient
$T_1, T_2, T_3,$ T_4, T_∞	temperature		

process are not easy to obtain due to the complication of the three-dimensional case and the fact that the value at the interfacial boundary between layers is unknown. Only a few studies have considered these kinds of problems in the literature [1, 2, 6, 9, 10]. Recently, Dai and Nassar [19, 20] have developed numerical heat transfer models for thermal analysis in X-ray irradiated photoresists. The steady state temperature distribution in the resist has been obtained by solving the unsteady state differential equations in the case of two layers, resist and substrate, with rectangular or cylindrical geometry. In this article, we develop a preconditioned Richardson method to investigate the steady state temperature distribution in a commercially applicable X-ray irradiation process with cylindrical geometry, where the target consists of a mask, a resist, and a substrate (with a gap between mask and resist). In this method, a hybrid finite element–finite difference scheme combined with a preconditioned Richardson method will be applied for solving the Poisson equation at the microscale to obtain the steady state temperature. A domain decomposition algorithm is then developed based on a parallel Gaussian elimination for solving block tridiagonal linear systems, which overcomes the problem with the unknown value at the interface. Such a method is simple and fast, as compared with previous methods.

X-RAY IRRADIATION PROCESS

We now consider a commercially applicable X-ray irradiation process with cylindrical geometry, where the target consists of a mask, a resist, and a substrate (with a gap between mask and resist), as shown in Figure 1 (mask, resist, and substrate are held in place through a special clamping mechanism not shown in the figure). A gap exists between mask and resist through which air circulates to prevent overheating on the exposed area of the resist. The resist such as PMMA is placed on a substrate such as silicon. The cylindrical mask, resist, and substrate are very thin, of the order of 300, 300, and 500 μm, respectively, with a radius of 5 mm. The gap is also very thin, of the order of 50 μm. To study the effect of the high-flux X-ray exposure on distortions in the resist, it is important to predict the temperature distribution in the resist and the substrate. Heat from the X-ray beam is first transferred by conduction through the mask. Due to the very thin gap and the relatively low temperature, radiation can be neglected. Also, convection in the gap is small relative to conduction. Hence, without loss of generality, we assume that heat is mainly transferred by conduction through the gap. Heat is then transferred by conduction through the resist and substrate. As such, the governing

equations for temperatures at steady state in the mask, gap, resist, and substrate are given by the elliptic equations [1, 21, 22]:

Mask

$$-k_1\left(\frac{\partial^2 T_1}{\partial x^2}+\frac{\partial^2 T_1}{\partial y^2}+\frac{\partial^2 T_1}{\partial z^2}\right)=g_1(x,y,z) \tag{1}$$

Gap

$$-k_2\left(\frac{\partial^2 T_2}{\partial x^2}+\frac{\partial^2 T_2}{\partial y^2}+\frac{\partial^2 T_2}{\partial z^2}\right)=g_2(x,y,z) \tag{2}$$

Resist

$$-k_3\left(\frac{\partial^2 T_3}{\partial x^2}+\frac{\partial^2 T_3}{\partial y^2}+\frac{\partial^2 T_3}{\partial z^2}\right)=g_3(x,y,z) \tag{3}$$

Substrate

$$-k_4\left(\frac{\partial^2 T_4}{\partial x^2}+\frac{\partial^2 T_4}{\partial y^2}+\frac{\partial^2 T_4}{\partial z^2}\right)=g_4(x,y,z) \tag{4}$$

where T_1, T_2, T_3, T_4 are temperatures, and k_1, k_2, k_3, k_4 are conductivities. The source term $g_i(x, y, z)(i = 1, 2, 3, 4)$ depends on the mode of the system and can be determined by experiments. The boundary conditions are described as follows.

On the top surface of the mask, $z = 0$, where heat convection occurs,

$$k_1\frac{\partial T_1}{\partial z}=h_c(T_1-T_\infty) \tag{5}$$

where T_∞ is the temperature of the surroundings and h_c is the convection coefficient.

On the bottom surface of the mask, $z = H_1$, we assume that the flux across the interface does not change:

$$-k_1\frac{\partial T_1}{\partial z}=-k_2\frac{\partial T_2}{\partial z} \qquad T_1=T_2 \tag{6}$$

Similarly, on the top surface of the resist, $z = H_1 + H_2$,

$$-k_2\frac{\partial T_2}{\partial z}=-k_3\frac{\partial T_3}{\partial z} \qquad T_3=T_2 \tag{7}$$

On the bottom surface of the resist, $z = H_1 + H_2 + H_3$,

$$-k_3\frac{\partial T_3}{\partial z}=-k_4\frac{\partial T_4}{\partial z} \qquad T_3=T_4 \tag{8}$$

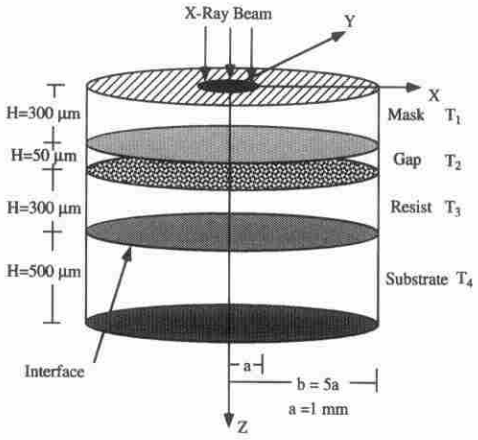

Figure 1. Three-dimensional configuration of mask, gap, resist and substrate.

Under experimental conditions, the side walls of the mask, resist, and substrate (Figure 1) and the bottom surface of the substrate are kept at a constant temperature or open to the surroundings, so as to prevent heat from building up. As such, it is realistic to assume $T_i = T_\infty$, $i = 1, 2, 3, 4$, on the side walls, and $T_4 = T_\infty$ on the bottom surface of the substrate.

NUMERICAL MODEL

The numerical model is developed based on a hybrid finite element–finite difference scheme, and a precondition Richardson method for the Poisson equation at the microscale. A domain decomposition algorithm is then obtained based on a parallel Gaussian elimination technique for solving block tridiagonal systems. To this end, we first apply the finite element method for the xy cross section.

Consider

$$-k\left(\frac{\partial^2 T}{\partial x^2} + \frac{\partial^2 T}{\partial y^2} + \frac{\partial^2 T}{\partial z^2}\right) = g(x, y, z) \tag{9}$$

with $T = 0$ when the point (x, y, z) is on the side wall. Let

$$\begin{aligned}
&\iint_G \left[-k\left(\frac{\partial^2 T}{\partial x^2} + \frac{\partial^2 T}{\partial y^2} + \frac{\partial^2 T}{\partial z^2}\right)\nu - g\nu\right] dx\,dy \\
&\quad = \iint_G \left[k\left(\frac{\partial T}{\partial x}\frac{\partial \nu}{\partial x} + \frac{\partial T}{\partial y}\frac{\partial \nu}{\partial y}\right) - k\frac{\partial^2 T}{\partial z^2}\nu - g\nu\right] dx\,dy \\
&\quad = 0 \qquad \nu \in H_0^1
\end{aligned} \tag{10}$$

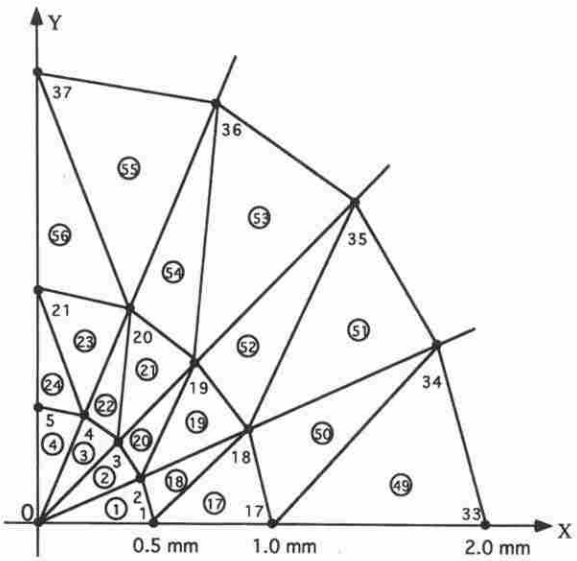

Figure 2. Part of the finite element mesh in the xy cross section.

where $\nu(x, y)$ is a function in the Sobolev space H_0^1 [23]. A finite element mesh is constructed in the xy cross section, as shown in Figure 2. In each element, as shown in Figure 3, we choose a linear basis function

$$\varphi_p = L_p = \frac{1}{2S_\Delta}(a_p + b_p x + c_p y) \tag{11}$$

where $a_p = x_q y_r - x_r y_q$, $b_p = y_q - y_r$, $c_p = x_r - x_q$, and

$$2S_\Delta = \frac{1}{2}\left[x_p(y_q - y_r) + x_q(y_r - y_p) + x_r(y_p - y_q)\right] \tag{12}$$

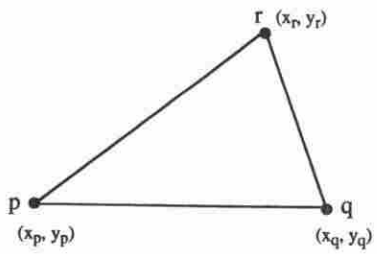

Figure 3. A triangular element Δ.

Then a test function for $T(x, y, z)$ can be written as

$$T_h(x, y, z) = \sum_{p=1}^{N} T_p(z)\varphi_p(x, y) \tag{13}$$

where N is the number of grid points in the xy cross section. Also, we consider

$$g_h = \sum_{p=1}^{N} g_p \varphi_p(x, y)$$

as an interpolant of g. Substituting $T_h(x, y, z)$ and g_h into Eq. (10), we obtain

$$\sum_{p=1}^{N}\left[kT_p\iint_G\left(\frac{\partial\varphi_p}{\partial x}\frac{\partial\nu}{\partial x}+\frac{\partial\varphi_p}{\partial y}\frac{\partial\nu}{\partial y}\right)dx\,dy - k\frac{\partial^2 T_p}{\partial z^2}\iint_G \varphi_p\nu\,dx\,dy\right]$$

$$-\sum_{p=1}^{N} g_p\iint_G \varphi_p\nu\,dx\,dy = 0 \tag{14}$$

If we choose $\nu = \varphi_q$, then Eq. (14) becomes

$$\sum_{p=1}^{N}\left[kT_p\iint_G\left(\frac{\partial\varphi_p}{\partial x}\frac{\partial\varphi_q}{\partial x}+\frac{\partial\varphi_p}{\partial y}\frac{\partial\varphi_q}{\partial y}\right)dx\,dy - k\frac{\partial^2 T_p}{\partial z^2}\iint_G \varphi_p\varphi_q\,dx\,dy\right]$$

$$-\sum_{p=1}^{N} g_p\iint_G \varphi_p\varphi_q\,dx\,dy = 0 \qquad q = 1, 2, \cdots, N \tag{15}$$

Introducing the vector notations $\vec{T}(z) = [T_1(z), \cdots, T_N(z)]^T$, $\vec{f}(z) = (g_1, \cdots, g_N)^T$ and the matrices $M_{N\times N}$ and $K_{N\times N}$ with the two respective entries,

$$m_{qp} = \iint_G \varphi_p\varphi_q\,dx\,dy \qquad k_{qp} = \iint_G\left(\frac{\partial\varphi_p}{\partial x}\frac{\partial\varphi_q}{\partial x}+\frac{\partial\varphi_p}{\partial y}\frac{\partial\varphi_q}{\partial y}\right)dx\,dy$$

we can express system Eq. (15) in matrix form as follows:

$$kK\vec{T} - kM\frac{\partial^2\vec{T}}{\partial z^2} = M\vec{f} \tag{16}$$

For simplification, we apply the lumped mass technique [23, 24] to obtain a diagonal matrix D and then replace M by D in Eq. (16) to give

$$kK\vec{T} - kD\frac{\partial^2\vec{T}}{\partial z^2} = D\vec{f} \tag{17}$$

where each entry d_i at the diagonal of D is $\frac{1}{3}\Sigma_\Delta S_\Delta$ (i.e., one-third of the sum of all elements with node i as one vertex).

We now develop a hybrid finite element–finite difference scheme. Let $\vec{T}_m = \vec{T}(m\Delta z)$, where Δz is the grid size in the z direction, $m = 1,\cdots, N_z$. Using a second-order standard finite difference to approximate $\partial^2\vec{T}/\partial z^2$, we obtain a discretized equation for Eq. (17) as follows:

$$kK\vec{T}_m - \lambda D\left(\vec{T}_{m+1} - 2\vec{T}_m + \vec{T}_{m-1}\right) = D\vec{f}_m \qquad m = 1,\cdots, N_z \tag{18}$$

where $\lambda = k/\Delta z^2$. Since K is a sparse matrix making the above system complex, the computation will be more complicated if Eqs. (1)–(4) are discretized using Eq. (18) with their discrete boundary and interfacial conditions. To simplify the system, we apply a preconditioned Richardson iteration based on the idea in Refs. [25, 26] with regard to Eq. (18). This gives

$$\begin{aligned} &kD_1\vec{T}_m^{(n+1)} - \lambda D\left(\vec{T}_{m+1}^{(n+1)} - 2\vec{T}_m^{(n+1)} + \vec{T}_{m-1}^{(n+1)}\right) \\ &\quad = kD_1\vec{T}_m^{(n)} - \lambda D\left(\vec{T}_{m+1}^{(n)} - 2\vec{T}_m^{(n)} + \vec{T}_{m-1}^{(n)}\right) \\ &\qquad - \beta\left[kK\vec{T}_m^{(n)} - \lambda D\left(\vec{T}_{m+1}^{(n)} - 2\vec{T}_m^{(n)} + \vec{T}_{m-1}^{(n)}\right) - D\vec{f}_m\right] \\ &m = 1,\cdots, N_z \qquad n = 1, 2, 3, \cdots \end{aligned} \tag{19}$$

where D_1 is a diagonal matrix with a diagonal entry, $d_i = 2k_{ii}$, k_{ii} is the entry on the main diagonal line of the matrix K, and $i = 1, 2,\cdots, N$. Here, β is a relaxation parameter. The advantage of the above preconditioned Richardson iteration is that it converges much faster in the microscale case (see discussion in Appendix A).

We now apply the precondition Richardson iteration in Eq. (19) to solve Eqs. (1)–(4) and write the scheme as follows:

e

$$\begin{aligned} &k_iD_1\left(\vec{T}_i\right)_m^{(n+1)} - \lambda_i D\left[\left(\vec{T}_i\right)_{m+1}^{(n+1)} - 2\left(\vec{T}_i\right)_m^{(n+1)} + \left(\vec{T}_i\right)_{m-1}^{(n+1)}\right] \\ &\quad = k_iD_1\left(\vec{T}_i\right)_m^{(n)} - \lambda_i D\left[\left(\vec{T}_i\right)_{m+1}^{(n)} - 2\left(\vec{T}_i\right)_m^{(n)} + \left(\vec{T}_i\right)_{m-1}^{(n)}\right] \\ &\qquad - \beta\left\{k_iK\left(\vec{T}_i\right)_m^{(n)} - \lambda_i D\left[\left(\vec{T}_i\right)_{m+1}^{(n)} - 2\left(\vec{T}_i\right)_m^{(n)} + \left(\vec{T}_i\right)_{m-1}^{(n)}\right] - D\left(\vec{f}_i\right)_m\right\} \\ &m = 1,\cdots, N_z^i \qquad n = 1, 2, 3, \cdots \end{aligned} \tag{20}$$

where $i = 1, 2, 3, 4$. At each iteration step, $(\vec{T}_i)_m^{(n+1)}$ is assumed to satisfy the discrete boundary and interfacial conditions as follows:

$$k_1 \frac{\left(\vec{T}_1\right)_1^{(n+1)} - \left(\vec{T}_1\right)_0^{(n+1)}}{\Delta z_1} = h_c\left[\left(\vec{T}_1\right)_0^{(n+1)} - \vec{T}_\infty\right] \qquad z = 0 \tag{21a}$$

$$-k_1 \frac{\left(\vec{T}_1\right)_{N_z^1+1}^{(n+1)} - \left(\vec{T}_1\right)_{N_z^1}^{(n+1)}}{\Delta z_1} = -k_2 \frac{\left(\vec{T}_2\right)_1^{(n+1)} - \left(\vec{T}_2\right)_0^{(n+1)}}{\Delta z_2} \qquad z = H_1 \tag{21b}$$

$$\left(\vec{T}_1\right)_{N_z^1+1}^{(n+1)} = \left(\vec{T}_2\right)_0^{(n+1)}$$

$$-k_2 \frac{\left(\vec{T}_2\right)_{N_z^2+1}^{(n+1)} - \left(\vec{T}_2\right)_{N_z^2}^{(n+1)}}{\Delta z_2} = -k_3 \frac{\left(\vec{T}_3\right)_1^{(n+1)} - \left(\vec{T}_3\right)_0^{(n+1)}}{\Delta z_3} \qquad z = H_1 + H_2 \tag{21c}$$

$$\left(\vec{T}_2\right)_{N_z^2+1}^{(n+1)} = \left(\vec{T}_3\right)_0^{(n+1)}$$

$$-k_3 \frac{\left(\vec{T}_3\right)_{N_z^3+1}^{(n+1)} - \left(\vec{T}_3\right)_{N_z^3}^{(n+1)}}{\Delta z_3} = -k_4 \frac{\left(\vec{T}_4\right)_1^{(n+1)} - \left(\vec{T}_4\right)_0^{(n+1)}}{\Delta z_4} \qquad z = H_1 + H_2 + H_3$$

$$\left(\vec{T}_3\right)_{N_z^3+1}^{(n+1)} = \left(\vec{T}_4\right)_0^{(n+1)} \tag{21d}$$

On the other boundaries,

$$\left(\vec{T}_i\right)_m^{(n+1)} = T_\infty \qquad i = 1, 2, 3, 4 \tag{21e}$$

The $\{(\vec{T}_i)_m^{(n+1)}\}(i = 1, 2, 3, 4)$ are computed by Eq. (20). As such, we express these equations as four block tridiagonal linear systems:

$$-\lambda_i D\left(\vec{T}_i\right)_{m-1}^{(n+1)} + (2\lambda_i D + k_i D_1)\left(\vec{T}_i\right)_m^{(n+1)} - \lambda_i D\left(\vec{T}_i\right)_{m+1}^{(n+1)} = \left(\vec{c}_i\right)_m^{(n)}$$

$$m = 1, \cdots, N_z^i \tag{22}$$

where $i = 1, 2, 3, 4$. Since $\{(\vec{T}_i)_m^{(n+1)}\}(i = 1, 2, 3, 4)$ is unknown at the interface between layers, the above four block tridiagonal linear systems cannot be solved. To overcome this difficulty, we apply a parallel Gaussian elimination (described in Appendix B) for solving block tridiagonal linear systems. As such, a domain decomposition algorithm for thermal analysis in the X-ray irradiation process can be described as follows.

Step 1: calculate the coefficients as listed in step 1 of the parallel Gaussian elimination (Appendix B).

Step 2: substitute the following six equations:

$$\left(\vec{T}_1\right)_{N_z^1}^{(n+1)} = A_{N_z^1}^{(1)}\left(\vec{T}_1\right)_{N_z^1+1}^{(n+1)} + \vec{\mathbf{v}}_{N_z^1}^{(1)}$$

$$\left(\vec{T}_2\right)_{N_z^2}^{(n+1)} = A_{N_z^2}^{(2)}\left(\vec{T}_2\right)_{N_z^2+1}^{(n+1)} + \vec{\mathbf{v}}_{N_z^2}^{(2)} + \vec{\mathbf{w}}_{N_z^2}^{(2)}\left(\vec{T}_2\right)_0^{(n+1)}$$

$$\left(\vec{T}_2\right)_1^{(n+1)} = \tilde{A}_1^{(2)}\left(\vec{T}_2\right)_0^{(n+1} + \tilde{\mathbf{v}}_1^{(2)} + \tilde{\mathbf{w}}_1^{(2)}\left(\vec{T}_2\right)_{N_z^2+1}^{(n+1)}$$

$$\left(\vec{T}_3\right)_{N_z^3}^{(n+1)} = A_{N_z^3}^{(3)}\left(\vec{T}_3\right)_{N_z^3+1}^{(n+1)} + \vec{\mathbf{v}}_{N_z^3}^{(3)} + \vec{\mathbf{w}}_{N_z^3}^{(3)}\left(\vec{T}_3\right)_0^{(n+1)}$$

$$(T_3)_1^{(n+1)} = \tilde{A}_1^{(3)}\left(\vec{T}_3\right)_0^{(n+1)} + \tilde{\mathbf{v}}_1^{(3)} + \tilde{\mathbf{w}}_1^{(3)}\left(\vec{T}_3\right)_{N_z^3+1}^{(n+1)}$$

$$\left(\vec{T}_4\right)_1^{(n+1)} = \tilde{A}_1^{(4)}\left(\vec{T}_4\right)_0^{(n+1)} + \tilde{\mathbf{v}}_1^{(4)}$$

into the discrete boundary equations, Eqs. (21*b*)–(21*d*), to obtain $(\vec{T}_1)_{N_z^1+1}^{(n+1)}$, $(\vec{T}_2)_0^{(n+1)}$, $(\vec{T}_2)_{N_z^2+1}^{(n+1)}$, $(\vec{T}_3)_0^{(n+1)}$, $(\vec{T}_3)_{N_z^3+1}^{(n+1)}$, and $(\vec{T}_4)_0^{(n+1)}$.

Step 3: solve for the rest of the unknowns in $\{(\vec{T}_i)_m^{(n+1)}\}(i = 1, 2, 3, 4)$ by step 3 of the parallel Gaussian elimination.

The above iterations are continued until a criterion for convergence is satisfied.

NUMERICAL RESULTS

To demonstrate the applicability of the present numerical method, we investigate the maximum temperature rise in the resist. Two examples are illustrated below.

The first example is to compare the present method with our previous method for obtaining the steady state temperature by solving the unsteady state differential equations (see [20]). In this example, we only considered the resist and substrate case and assumed that the thickness of each resist and substrate was 100 μm, as shown in Figure 4. PMMA and silicon were used as the resist and substrate, respectively. We followed the assumption in Ref. [1] that the resist and substrate have a linear absorption coefficient μ and are uniformly exposed with an irradiance W_0. A commonly used model for heat absorption is the exponential expression [1]

$$g(x, y, z) = \begin{cases} W_0 \mu e^{-\mu z} & 0 \leqslant r \leqslant a \\ 0 & a < r \leqslant b \end{cases} \tag{23}$$

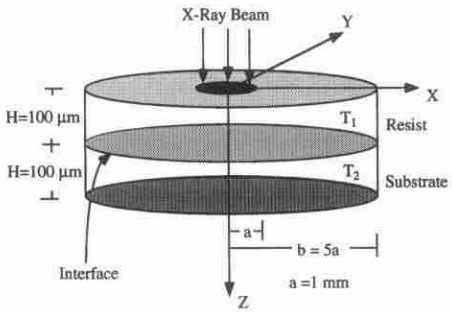

Figure 4. Three-dimensional configuration of resist and substrate.

where the coefficients W_0 and μ were chosen to be 3.4 W/cm^2 and $(1/106) \times 10^4$/cm, respectively. This expression shows that heat absorbed from the synchrotron X-ray irradiating the surface decreases exponentially with depth. A convection coefficient $h_c = 0.006$ W/cm^2/K was chosen for the top of the resist. Conductivities of PMMA and silicon used in the analysis are listed in Table 1. We considered the same finite element mesh as that in Ref. [20] with 97 grid points in the xy cross section (Figure 2) and chose 50 grid points in the z direction for each layer. The convergent solution was obtained when $\max|T^{(n+1)} - T^{(n)}| \leqslant 0.5 \times 10^{-3}$ was satisfied in the resist, which is the same as that in Ref. [20].

Based on the above parameters, the solution obtained gave a maximum temperature rise within the resist of 5.736 K at the center when $n = 8$ and $\beta = 0.95$. This result is very close to 5.728 K obtained in Ref. [20].

More details of the temperature field can be obtained from the three-dimensional model. Figure 5 shows the temperature profile along the central line in the z direction. This profile agreed well with the temperature profile in Ref. [20]. Further, Figure 6 shows contours of the temperature distributions in the rz cross section in the resist, which is similar to that obtained in Ref. [20].

The CPU times for the present method and for the splitting method in Ref. [20] were compared using a SUN workstation. It took about 10 s to obtain the steady state solution with the present method. On the other hand, 7.5 min were required using the splitting method.

We tested the efficiency with regard to the relaxation parameter β, as listed in Table 2. Results show that the iteration number n becomes small as β approaches 1. This result coincides with the theoretical analysis in Appendix A.

The second example deals with an implementation of the present method to a commercially applicable X-ray irradiation process, where the target consists of a mask, a resist, and a substrate (with a gap between mask and resist), as shown in Figure 1. In this example, beryllium, He gas, PMMA, and silicon were used for the mask, gap, resist, and substrate, respectively. The heat absorption in each layer is the exponential expression

$$g_i(x, y, z) = \begin{cases} (W_0)_i(\mu)_i e^{-(\mu)_i z} & 0 \leqslant r \leqslant a \\ 0 & a < r \leqslant b \end{cases} \qquad i = 1, 2, 3, 4 \tag{24}$$

Table 1. Parameters used for the different layers

Properties	Beryllium [27]	He gas (100 mbar) [28]	PMMA [29]	Silicon [27]
k, W/cm/K	2.0	0.00152	0.00198	1.5
W_0, W/cm^2	2.042	0.0	1.823	1.424
μ, cm^{-1}	40.81	0.0	50.26	99.42

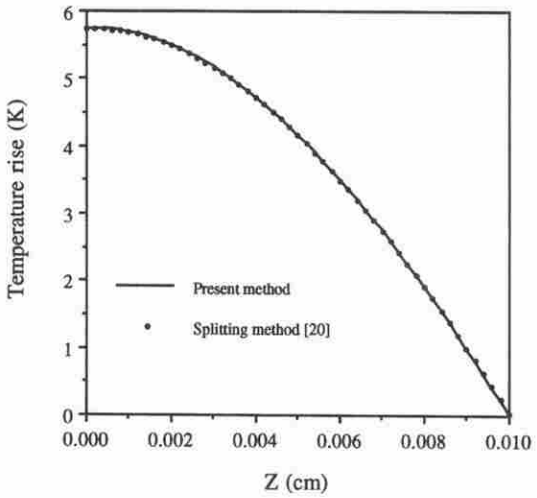

Figure 5. Temperature profiles along the z axis where the maximum temperature rise occurs in the resist.

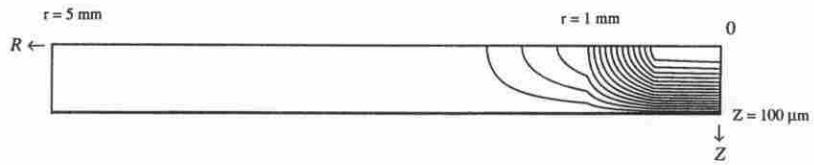

Figure 6. Contour of the temperature distribution for the resist in the rz cross section.

Table 2. Number of iterations as a function of the relaxation parameter β for the first example

β	n
0.95	8
0.90	9
0.80	10

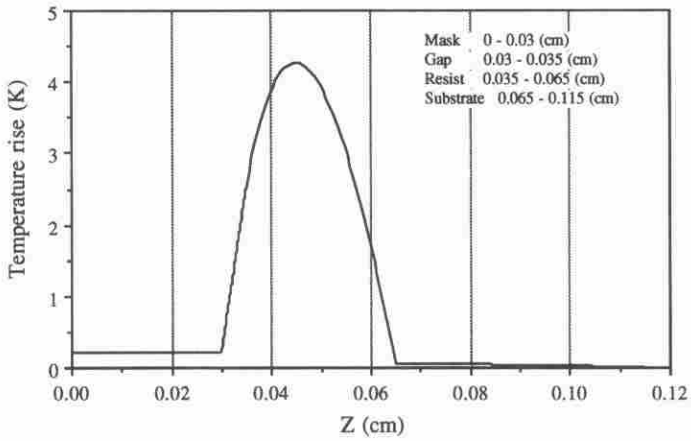

Figure 7. Temperature profiles along the z axis where the maximum temperature rise occurs in the resist.

where the coefficients W_0 and μ for the mask, gap, resist, and substrate were chosen as listed in Table 1 [27–29]. For convenience, we take the exposed area to be circular (with radius $r = a$) and in the center of the mask (Figure 1). However, it should be noted that in general, this area may not be in the center. Hence it is necessary to consider a three-dimensional model. Furthermore, we chose a convection coefficient $h_c = 0.006$ W/cm^2/K for the top of the mask. We considered a finite element mesh with the same 97 grid points in the xy cross section, as shown in Figure 2, for each layer, and chose 50 grid points in the z direction for mask, gap, resist, and substrate, respectively. The convergent solution was obtained when $\max|(T^{(n+1)} - T^{(n)}/T^{(n+1)}| \leqslant 1.0\%$ was satisfied in the resist.

Based on the above parameters, the solution obtained gave a maximum temperature rise within the resist of 4.36 K at the center when $n = 93$ and $\beta = 0.95$ with a CPU time of about 3 min in a SUN workstation. Figure 7 shows the temperature profile along the central line in the z direction. Figure 8 shows contours of the temperature distributions on the rz cross section.

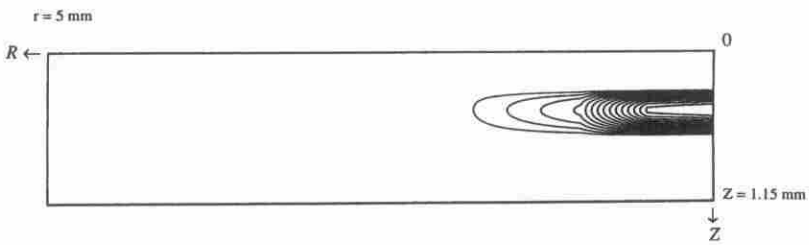

Figure 8. Contour of the temperature distribution in the rz cross section.

Table 3. Number of iterations as a function of the relaxation parameter β for the second example

β	n
0.95	93
0.90	95
0.80	100

We also tested the efficiency with regard to the relaxation parameter β, as listed in Table 3. Again, results show that the iteration number n becomes small as β approaches 1. This result also coincides with the theoretical analysis in Appendix A.

CONCLUSION

The temperature distribution in an X-ray lithography with cylindrical geometry is modeled with the three-dimensional steady state heat equations. A numerical solution is obtained using a hybrid finite element–finite difference scheme, and a preconditioned Richardson method for solving the Poisson equation at the microscale. A domain decomposition algorithm is obtained by implementing a parallel Gaussian elimination technique. Results reflected accurately the temperature profiles as well as the maximum temperature rise in the photoresist. The numerical procedure is simple and fast and overcomes the unknown at the interface between layers. The present numerical model is suitable for three-dimensional multilayer investigations in X-ray lithography where an analytic solution is difficult to obtain. It can be applied to experimental situations in multilayers (mask, resist, substrate, and gap between mask and resist) with arbitrary geometry and source conditions. It is known that scan length and speed affect the temperature rise in the resist. In future work, we will consider arbitrary geometry and continuous scanning of the wafer/mask assembly across the synchrotron radiation beam.

REFERENCES

1. T. A. Ameel, R. O. Warrington, D. Yu, and G. Dahlbacka, Thermal Analysis of X-Ray Irradiated Thick Resists to Determine Induced Structural Deformations, *Heat Transfer*, vol. 4, pp. 313–318, 1994.
2. K. D. Cole and W. A. McGahan, Theory of Multilayers Heated by Laser Absorption, *J. Heat Transfer*, vol. 115, pp. 767–771, 1993.
3. L. A. Dillon et al., Surface Temperature Measurements Using a Thin Film Thermal Array, *NASA Tech. Memo.*, TM 101549, 1989.
4. G. Feiertag, M. Schmidt, and A. Schmidt, Thermoelastic Deformations of Masks for Deep X-Ray Lithography, *Microelectron. Eng.*, vol. 27, pp. 513–516, 1995.
5. G. Feiertag et al., Accuracy of Structure Transfer in Deep X-Ray Lithograph, *Microelectron. Eng.*, vol. 35, pp. 557–560, 1997.

6. R. Kant, Laser-Induced Heating of a Multilayered Medium Resting on a Half-Space: Part I—Stationary Source, *J. Appl. Mech.*, vol. 55, pp. 93–97, 1988.
7. D. L. Laird et al., Analysis and Optimization of X-Ray Masks Using Finite Element Methods, *Microelectron. Eng.*, vol. 17, pp. 209–214, 1992.
8. D.-C. Li et al., Computer Simulations for Mask Structure Heating in X-Ray Lithography, *Comput. Structures*, vol. 58, pp. 825–834, 1996.
9. M. R. Madison and T. W. McDaniel, Temperature Distributions Produced in an *N*-Layer by Static or Scanning Laser or Electron Beam with Application to Magneto-Optical Media, *J. Appl. Phys.*, vol. 66, pp. 5738–5748, 1989.
10. H. M. Manohara et al., Temperature Rise in Thick PMMA Resists During X-Ray Exposure, *Proc. SPIE Int. Soc. Opt. Eng.*, vol. 2880, p. 183, 1996.
11. I. A. Shareef et al., Thermoelastic Behavior of X-Ray Lithography Masks During Irradiation, *IBM J. Res. Dev.*, vol. 34, pp. 718–735, 1990.
12. Y. Vladimirsky et al., Thermal Effects in X-Ray Mask During Synchrotron Storage Ring Irradiation, *J. Vac. Sci. Technol. B*, vol. 7, no. 6, pp. 1657–1661, 1989.
13. Y. Vladimirsky et al., Thermoelastic Effects in X-Ray Lithography Masks During Synchrotron Storage Ring Irradiation, *Microelectron. Eng.*, vol. 11, pp. 287–293, 1990.
14. Y. Vladimirsky et al., Thin Metal Film Thermal Micro-Sensors, *Proc. SPIE Int. Soc. Opt. Eng.*, vol. 2640, p. 184, 1995.
15. Y. Vladimirsky et al., X-Ray Lithography Program at the Center for Advanced Microstructures and Devices, *Proc. Electrochem. Soc.*, vol. 95-18, p. 366, 1995.
16. Y. Vladimrsky et al., X-Ray Micro-Lithography Exposure System for High Aspect Ratio Micromachining, *Proc. SPIE Int. Soc. Opt. Eng.*, vol. 2640, p. 36, 1995.
17. O. Vladimirsky et al., Thick PMMA Layer Formation as an X-Ray Imaging Medium for Micromachining, *Proc. SPIE Int. Soc. Opt. Eng.*, vol. 2723, 1996.
18. H. Zumaque, G. A. Kohring, and J. Hormes, Simulation Studies of Energy Deposition and Secondary Processes in Deep X-Ray Lithography, *J. Micromech. Microeng.*, vol. 7, pp. 79–88, 1997.
19. W. Dai, R. Nassar, R. O. Warrington, and B. Shen, Three-Dimensional Numerical Models for Thermal Analysis in X-Ray Irradiated Photoresists, *Numer. Heat Transfer Part A*, vol. 31, pp. 585–595, 1997.
20. W. Dai and R. Nassar, A Three-Dimensional Numerical Model for Thermal Analysis in X-Ray Irradiated Photoresists with Cylindrical Domain, *Numer. Heat Transfer Part A*, vol. 32, pp. 517–530, 1997.
21. F. P. Incropera and D. P. Dewitt, *Fundamentals of Heat and Mass Transfer*, 2nd ed., John Wiley, New York, 1985.
22. M. N. Ozisik, *Heat Conduction*, John Wiley, New York, 1980.
23. T. R. Chandrupatla and A. D. Belegundu, *Introduction to Finite Elements in Engineering*, pp. 334–371, Prentice-Hall, Englewood Cliffs, N.J., 1991.
24. G. F. Carey and J. T. Oden, *Finite Elements*, vol. 3, pp. 273–279, Prentice-Hall, Englewood Cliffs, N.J., 1984.
25. C. Canuto, M. Y. Hussaini, A. Quarteroni, and T. A. Zang, *Spectral Methods in Fluid Dynamics*, Springer-Verlag, New York, 1988.
26. M. O. Deville, E. H. Mund, and V. Van Kemenade, Preconditioned Chebyshev Collocation Methods and Triangular Finite Elements, *Comput. Methods Appl. Mech. Eng.*, vol. 16, pp. 193–200, 1994.
27. R. C. Weast, *1985-86 CRC Handbook of Chemistry and Physics*, 66th ed., pp. B9, B34, D178–179, E11, E13, CRC Press, Boca Raton, Fla., 1985.
28. R. F. Barron, *Cryogenic Systems*, 2nd ed., p. 481, Oxford University Press, New York, 1985.

29. J. Brandup and E. H. Immergut, *Polymer Handbook*, 3rd ed., pp. V/77–79, John Wiley, New York, 1989.
30. K. E. Atkinson, *An Introduction to Numerical Analysis*, 2nd ed., John Wiley, New York, 1988.
31. H. Anton, *Elementary Linear Algebra*, 7th ed., Wiley, New York, 1994.
32. J. M. Ottega, *Introduction to Parallel and Vector Solution of Linear Systems*, Plenum Press, New York, 1988.

APPENDIX A

Introduce the following notations for matrices and vectors,

$$\mathbf{K} = \begin{bmatrix} K & & \\ & \ddots & \\ & & K \end{bmatrix} \quad \mathbf{D} = \begin{bmatrix} D & & \\ & \ddots & \\ & & D \end{bmatrix} \quad \mathbf{D}_1 = \begin{bmatrix} D_1 & & \\ & \ddots & \\ & & D_1 \end{bmatrix}$$

$$\mathbf{U} = \begin{bmatrix} 2D & -D & & & \\ -D & 2D & -D & & \\ & & \ddots & & \\ & & -D & 2D & -D \\ & & & -D & 2D \end{bmatrix} \quad \vec{\mathbf{F}} = \begin{bmatrix} \vec{f}_1 \\ \vdots \\ \vec{f}_{Nz} \end{bmatrix} \quad \vec{\mathbf{T}} = \begin{bmatrix} \vec{T}_1 \\ \vdots \\ \vec{T}_{Nz} \end{bmatrix}$$

$$\mathbf{L}_{\mathbf{pre}} = k\mathbf{D}_1 + \frac{k}{\Delta z^2}\mathbf{U} \qquad \mathbf{A} = k\mathbf{K} + \frac{k}{\Delta z^2}\mathbf{U}$$

we can rewrite Eq. (19) in matrix form as follows:

$$\mathbf{L}_{\mathbf{pre}}\vec{\mathbf{T}}^{(\mathbf{n}+1)} = \mathbf{L}_{\mathbf{pre}}\vec{\mathbf{T}}^{(\mathbf{n})} - \beta\left(\mathbf{A}\vec{\mathbf{T}}^{(\mathbf{n})} - \mathbf{D}\vec{\mathbf{F}}\right) \tag{A1}$$

It is well known from numerical linear algebra [30] that the iteration process converges if the iteration operator $\mathbf{B} = \mathbf{I} - \beta\mathbf{L}_{\mathbf{pre}}^{-1}\mathbf{A}$ has a spectral radius $\rho(\mathbf{B}) < 1$. Further, the smaller $\rho(\mathbf{B})$ is, the faster the iteration converges. Let ξ be an eigenvalue of $\mathbf{L}_{\mathbf{pre}}^{-1}\mathbf{A}$ and $\vec{\mathbf{x}}$ be an eigenvector corresponding to ξ such that $\mathbf{A}\vec{\mathbf{x}} = \xi\mathbf{L}_{\mathbf{pre}}\vec{\mathbf{x}}$. Thus, ξ can be obtained as follows:

$$\xi = \frac{\vec{\mathbf{x}}^{\mathbf{T}}\mathbf{A}\vec{\mathbf{x}}}{\vec{\mathbf{x}}^{\mathbf{T}}\mathbf{L}_{\mathbf{pre}}\vec{\mathbf{x}}} = \frac{\vec{\mathbf{x}}^{\mathbf{T}}\mathbf{K}\vec{\mathbf{x}} + (1/\Delta z^2)\vec{\mathbf{x}}^{\mathbf{T}}\mathbf{U}\vec{\mathbf{x}}}{\vec{\mathbf{x}}^{\mathbf{T}}\mathbf{D}_1\vec{\mathbf{x}} + (1/\Delta z^2)\vec{\mathbf{x}}^{\mathbf{T}}\mathbf{U}\vec{\mathbf{x}}} \tag{A2}$$

Since K is symmetric and positive definite, $\mathbf{D}_1$ and $\mathbf{K}$ are symmetric and positive definite. Further, from the entry

$$k_{ii} \geqslant \sum_{\substack{j=1 \\ i \neq j}}^{N} |k_{ij}|$$

we obtain by the Gerschgorin theorem [30] that the eigenvalue σ_i of K satisfies

$$|\sigma_i - k_{ii}| \leqslant \sum_{\substack{j=1 \\ i \neq j}}^{N} |k_{ij}| \leqslant k_{ii} \quad \text{or} \quad 2k_{ii} - \sigma_i \geqslant 0$$

Thus we conclude from linear algebra [31] that $D_1 - K$ and hence $\mathbf{D}_1 - \mathbf{K}$ are symmetric and positive semidefinite. This results in $\vec{\mathbf{x}}^{\mathbf{T}}\mathbf{K}\vec{\mathbf{x}} \leqslant \vec{\mathbf{x}}^{\mathbf{T}}\mathbf{D}_1\vec{\mathbf{x}}$. Furthermore, since the size in the z direction is considered to be microscale, the dominating term in Eq. (A2) will be $(1/\Delta z^2)\vec{\mathbf{x}}^{\mathbf{T}}\mathbf{U}\vec{\mathbf{x}}$ if Δz is very small as compared to the grid size in the xy cross section. Hence we obtain from Eq. (A2) that $\xi \leqslant 1$ and is close to 1. If the relaxation parameter β is chosen to be less than but close to 1, then the spectral radius $\rho(\mathbf{B})$ will be close to zero. We conclude that the preconditioned Richardson iteration, Eq. (A1), will converge very quickly.

APPENDIX B

We consider a block tridiagonal linear system, which comes from the preconditioned Richardson iteration in Eq. (18) as follows:

$$\begin{gathered} -\lambda D\vec{T}_{m-1} + (2\lambda D + kD_1)\vec{T}_m - \lambda D\vec{T}_{m+1} = \vec{c}_m \qquad m = 1,\cdots, N_z \\ \vec{T}_0 = \vec{T}_{N_z+1} = \vec{0} \end{gathered} \tag{B1}$$

The Gaussian elimination for solving the block tridiagonal system results in a procedure called the "divide and conquer" procedure, shown as follows [20, 30]:

$$A_m = [2\lambda D + kD_1 - \lambda DA_{m-1}]^{-1}\lambda D \qquad A_0 = \mathbf{0} \tag{B2a}$$

$$\vec{\mathbf{v}}_m = [2\lambda D + kD_1 - \lambda DA_{m-1}]^{-1}\left(\vec{c}_m + \lambda D\vec{\mathbf{v}}_{m-1}\right) \qquad \vec{\mathbf{v}}_0 = \vec{0} \qquad m = 1,\cdots, N_z \tag{B2b}$$

$$\vec{T}_m = A_m\vec{T}_{m+1} + \vec{\mathbf{v}}_m \qquad \vec{T}_{N_z+1} = \vec{0} \qquad m = N_z,\cdots, 1 \tag{B2c}$$

In the above procedure, $A_m, \vec{\mathbf{v}}_m$ are calculated from $m = 1$ to $m = N_z$, while $\vec{T}_m$ is computed from $m = N_z$ to $m = 1$. A similar procedure that is opposite in direction can be expressed as

$$\tilde{A}_m = \left[2\lambda D + kD_1 - \lambda D\tilde{A}_{m+1}\right]^{-1}\lambda D \qquad \tilde{A}_{N_z+1} = \mathbf{0} \tag{B3a}$$

$$\tilde{\mathbf{v}}_m = \left[2\lambda D + kD_1 - \lambda D\tilde{A}_{m+1}\right]^{-1}\left(\vec{c}_m + \lambda D\tilde{\mathbf{v}}_{m+1}\right) \qquad \tilde{\mathbf{v}}_{N_z+1} = \vec{0} \qquad m = N_z,\cdots, 1 \tag{B3b}$$

$$\vec{T}_m = \tilde{A}_m\vec{T}_{m-1} + \tilde{\mathbf{v}}_m \qquad \vec{T}_0 = \vec{0} \qquad m = 1,\cdots, N_z \tag{B3c}$$

Further, if $\vec{T}_0$ and $\vec{T}_{N_z+1}$ are not zero, we have

$$A_m = [2\lambda D + kD_1 - \lambda D A_{m-1}]^{-1} \lambda D \qquad A_0 = \mathbf{0} \tag{B4a}$$

$$\vec{\mathbf{v}}_m = [2\lambda D + kD_1 - \lambda D A_{m-1}]^{-1} \left(\vec{c}_m + \lambda D \vec{\mathbf{v}}_{m-1}\right) \qquad \vec{\mathbf{v}}_0 = \vec{0} \tag{B4b}$$

$$\vec{\mathbf{w}}_m = [2\lambda D - kD_1 - \lambda D A_{m-1}]^{-1} \lambda D \vec{\mathbf{w}}_{m-1} \qquad \vec{\mathbf{w}}_0 = \vec{1} \qquad m = 1, \cdots, N_z \tag{B4c}$$

$$\vec{T}_m = A_m \vec{T}_{m+1} + \vec{\mathbf{v}}_m + \vec{\mathbf{w}}_m \vec{T}_0 \qquad m = N_z, \cdots, 1 \tag{B4d}$$

and

$$\tilde{A}_m = \left[2\lambda D + kD_1 - \lambda D \tilde{A}_{m+1}\right]^{-1} \lambda D \qquad \tilde{A}_{N_z+1} = \mathbf{0} \tag{B5a}$$

$$\tilde{\mathbf{v}}_m = \left[2\lambda D + kD_1 - \lambda D \tilde{A}_{m+1}\right]^{-1} \left(\vec{c}_m + \lambda D \tilde{\mathbf{v}}_{m+1}\right) \qquad \tilde{\mathbf{v}}_{N_z+1} = \vec{0} \tag{B5b}$$

$$\tilde{\mathbf{w}}_m = \left[2\lambda D + kD_1 - \lambda D \tilde{A}_{m+1}\right]^{-1} \lambda D \tilde{\mathbf{w}}_{m+1} \qquad \tilde{\mathbf{w}}_{N_z+1} = \vec{1} \qquad m = N_z, \cdots, 1 \tag{B5c}$$

$$\vec{T}_m = \tilde{A}_m \vec{T}_{m-1} + \tilde{\mathbf{v}}_m + \tilde{\mathbf{w}}_m \vec{T}_{N_z+1} \qquad m = 1, \cdots, N_z \tag{B5d}$$

It should be pointed out that the above procedures involve many matrix inverse calculations. However, the computation is rather simple, since D and D_1 are diagonal matrices.

Let $N_z = 4M + 3$ for convenience. We divide the system Eq. (B1) into four subsystems, which consist of the first M equations, the second M equations, the third M equations, and the last M equations. The $(M + 1)$th, $(2M + 2)$th, and $(3M + 3)$th equations designate the interfacial equations. If the above four procedures are combined together, then a parallel Gaussian elimination can be obtained based on the idea of the domain decomposition method [20, 32] as follows.

Step 1: calculate

$A_m^{(1)}, \vec{\mathbf{v}}_m^{(1)}$ $\quad m = 1, \cdots, M$, for the first M equations by (B2ab)

$A_m^{(2)}, \vec{\mathbf{v}}_m^{(2)}, \vec{\mathbf{w}}_m^{(2)}$ $\quad m = 1, \cdots, M$, for the second M equations by (B4abc)

$\tilde{A}_m^{(2)}, \tilde{\mathbf{v}}_m^{(2)}, \tilde{\mathbf{w}}_m^{(2)}$ $\quad m = M, \cdots, 1$, for the second M equations by (B5abc)

$A_m^{(3)}, \vec{\mathbf{v}}_m^{(3)}, \vec{\mathbf{w}}_m^{(3)}$ $\quad m = 1, \cdots, M$, for the third M equations by (B4abc)

$\tilde{A}_m^{(3)}, \tilde{\mathbf{v}}_m^{(3)}, \tilde{\mathbf{w}}_m^{(3)}$ $\quad m = M, \cdots, 1$, for the third M equations by (B5abc)

$\tilde{A}_m^{(4)}, \tilde{\mathbf{v}}_m^{(4)}$ $\quad m = M, \cdots, 1$, for the last M equations by (B3ab)

in parallel.

Step 2: substitute

$$\vec{T}_M = A_M^{(1)}\vec{T}_{M+1} + \mathbf{v}_M^{(1)} \qquad \vec{T}_{2M+1} = A_M^{(2)}\vec{T}_{2M+2} + \vec{\mathbf{v}}_M^{(2)} + \vec{\mathbf{w}}_M^{(2)}\vec{T}_{M+1}$$

$$\vec{T}_{M+2} = \tilde{A}_1^{(2)}\vec{T}_{M+1} + \tilde{\mathbf{v}}_1^{(2)} + \tilde{\mathbf{w}}_1^{(2)}\vec{T}_{2M+2} \qquad \vec{T}_{3M+2} = A_M^{(3)}\vec{T}_{3M+3} + \vec{\mathbf{v}}_M^{(3)} + \vec{\mathbf{w}}_M^{(3)}\vec{T}_{2M+2}$$

$$\vec{T}_{2M+3} = \tilde{A}_1^{(3)}\vec{T}_{2M+2} + \tilde{\mathbf{v}}_1^{(3)} + \tilde{\mathbf{w}}_1^{(3)}\vec{T}_{3M+3} \qquad \vec{T}_{3M+4} = \tilde{A}_1^{(4)}\vec{T}_{3M+3} + \tilde{\mathbf{v}}_1^{(4)}$$

into

$$-\lambda D\vec{T}_M + (2\lambda D + kD_1)\vec{T}_{M+1} - \lambda D\vec{T}_{M+2} = \vec{c}_{M+1}$$

$$-\lambda D\vec{T}_{2M+1} + (2\lambda D + kD_1)\vec{T}_{2M+2} - \lambda D\vec{T}_{2M+3} = \vec{c}_{2M+2}$$

$$-\lambda D\vec{T}_{3M+2} + (2\lambda D + kD_1)\vec{T}_{3M+3} - \lambda D\vec{T}_{3M+4} = \vec{c}_{3M+3}$$

then solve $\vec{T}_{M+1}$, $\vec{T}_{2M+2}$, and $\vec{T}_{3M+3}$.

Step 3: solve

$$\vec{T}_m = A_m^{(1)}\vec{T}_{m+1} + \vec{\mathbf{v}}_m^{(1)} \qquad m = M,\cdots,1$$

$$\vec{T}_{M+m+1} = A_m^{(2)}\vec{T}_{M+m+2} + \vec{\mathbf{v}}_m^{(2)} + \vec{\mathbf{w}}_m^{(2)}\vec{T}_{M+1} \qquad m = M,\cdots,1$$

$$\vec{T}_{2M+m+2} = A_m^{(3)}\vec{T}_{2M+m+3} + \vec{\mathbf{v}}_m^{(3)} + \vec{\mathbf{w}}_m^{(3)}\vec{T}_{2M+2} \qquad m = M,\cdots,1$$

$$\vec{T}_{3M+m+3} = \tilde{A}_m^{(4)}\vec{T}_{3M+m+2} + \tilde{\mathbf{v}}_m^{(4)} \qquad m = 1,\cdots,M$$

in parallel.